IEEE Access
Multidisciplinary | Rapid Review | Open Access Journal

Received April 25, 2020, accepted May 5, 2020, date of publication May 12, 2020, date of current version May 28, 2020.

Digital Object Identifier 10.1109/ACCESS.2020.2994064

A Wound-Field Pole-Changing Vernier Machine for Electric Vehicles

NOMAN BALOCH[1], SHAHID ATIQ[2], AND BYUNG-IL KWON[1], (Senior Member, IEEE)

[1]Department of Electrical and Electronic Engineering, Hanyang University, Ansan 15588, South Korea
[2]Electrical Engineering Department, Khwaja Fareed University of Engineering and Information Technology, Rahim Yar Khan 64200, Pakistan

Corresponding author: Byung-Il Kwon (bikwon@hanyang.ac.kr)

This work was supported in part by the BK21PLUS Program through the National Research Foundation of Korea within the Ministry of Education, and in part by the National Research Foundation of Korea (NRF) grant funded by the Korean government (Ministry of Science) (No. NRF-2020R1A2B5B01002400).

ABSTRACT This paper proposes a wound field pole changing vernier machine with fractional slot concentrated winding for electric vehicles application. The main aim of the paper is to utilize the advantages of a vernier machine and a wound field synchronous machine in a single topology using a fractional slot concentrated armature winding. The proposed machine operates in a vernier mode at low speeds and a wound-field synchronous mode at high speeds to utilize the merits of both a vernier machine and a wound-field synchronous machine. The topology, operating principle and pole-changing method of the proposed machine are explained initially. Then, finite element analysis (FEA) is utilized to study the electromagnetic characteristics such as back EMF, torque, wide speed range operation and efficiency of the proposed topology in two modes. Further, a prototype of the machine is manufactured and the FEA results are validated through experiments. The FEA and experiment results show that the proposed machine is a promising candidate for electric vehicles application.

INDEX TERMS Electric vehicles, pole changing, wound field synchronous machine, variable speed, vernier machine.

I. INTRODUCTION

The fluctuating prices of the fuel, the limited amount of the natural resources, and the global warming issues has led to massive energy efficiency and sustainability research. The electrification of vehicles is a serious issue in this regard because a large volume of oil is consumed by vehicles. Hence, the electric vehicle (EV) industry is expanding [1], [2]. The propulsion system of EVs has two major components that is electronic machines and the related power electronics equipment. The electric machines for EV application are required to operate on wide speed range and have high power density. Additionally, they must have high efficiency during wide speed range operation, high torque at low speeds for driving in urban areas and high power at high speeds for cruising [3], [5].

Most of these characteristics can be achieved by permanent-magnet (PM) synchronous machines and therefore, they have been actively used in EVs [6], [7]. There are two main classes of PM machines proposed for EV application: stator PM machines and rotor PM machines. The doubly-salient PM machine with hybrid excitation that incorporates the advantages of both switched reluctance and PM machine has been researched [8], [9]. The flux switching PM machines [10], [11] and flux reversal machines [12], [13] with PMs on the stator have also been proposed for EVs. Although their torque density is relatively low, but they have robust rotors. The interior permanent-magnet machines have high power density and high efficiency during wide speed range operation. Because of these characteristics they have been extensively proposed for EV application [14]–[16]. Moreover, memory machines and pole-changing machines, which can regulate the flux of low coercive PMs to extend the operating range of PM machines, have also been proposed [17]–[19].

Although the PM machines have been extensively used for EV application, they own high material costs and difficulty of PM flux control [20]–[22]. To overcome these drawbacks, many, PM efficient, rare-earth-free and PM-less topologies have been proposed [23]–[25]. PM efficient machines such as consequent pole PM machines have also been suggested and analyzed for in-wheel direct drive applications [23]. They

The associate editor coordinating the review of this manuscript and approving it for publication was Wei Xu.

present high torque per magnet volume but exhibit low overall power density. Further, their torque ripple is high due to additional harmonics. The electrical conductivity of ferrite PMs is lower than NdFeB magnets which leads to low eddy current losses. Additionally, ferrite PMs are much cheaper than NdFeB magnets. Rare-earth-free machines using ferrite magnets have been proposed and analyzed for automotive applications [24], [25].

Moreover, many PM-less topologies for EV application are available [26]; however, they each have their own demerits. The induction machines generally present low torque density [27], and the switched reluctance machines have low efficiency and high torque ripples [28], [29]. The wound-rotor synchronous machines have also been proposed for EVs [26], [30]–[33]. Since, there are no PMs in these machines, the rotors can be excited using different methods which have been discussed in detail in [34]. The most common method to excite the rotor is using a dc exciter through brushes and slip rings. Generally, the brushes often require maintenance and need to be replaced after a certain period of time. However, new brushes have been recently introduced which last much longer than conventional brushes and require less maintenance [35], [36]. Furthermore, brushless topologies such as using sub-harmonic [37] or 3rd harmonic excitation [38] have also been introduced which do not need brushes and slip rings. Wound-rotor machines present the advantages of high efficiency during wide speed range operation, good overload capability and great flux weakening control. Therefore, they have also been used in commercial electric vehicles such as Renault Zoe, which is discussed in [39]. However, they possess high copper losses leading to low efficiency during low speed operations. Further, these machines need large sizes of inverters in EV application. This is because EVs require high torque at low speed which is achieved by high stator and rotor currents in these machines.

The low-speed high-torque vernier machines have been proposed and analyzed broadly [40]–[43]. Because of their high torque density, they have been proposed for direct drive applications as well. Vernier machines usually exhibit high rotor pole pairs. The armature current frequency is also high which causes high reactance leading vernier machines to have a poor power factor [44]. Hence, an inverter with a high rating is generally required to drive the machine. Moreover, vernier machines also suffer from high core losses due to same high operating frequency. At high speeds, the operating frequency increases further leading to excessive core losses and therefore, low efficiency.

The efficiency of a vernier machine during wide speed range operations has not had much discussion. A PM vernier machine along with field winding in the stator slots is proposed to control the flux of the rotor PMs [45]. However, it suffers from limited fill factor for armature winding due to additional field winding in the stator slots. Moreover, the additional field winding adds to the weight of the machine. The field winding is moved in the slots between the flux modulation teeth to resolve the limited stator slots fill factor issue [46]. However, the field winding adds copper losses and also the power factor of the machine is poor in the high-speed region.

Wide speed range operation of vernier machines has also been achieved using winding switching [47]. However, winding switching requires two inverters and also the efficiency of vernier machines is low during wide speed range operation utilizing winding switching. A pole-changing vernier machine with two kind of PMs on the rotor has been presented for wide speed range operation [48]. Two types of PMs that is constant and low coercive force (LCF) magnets are incorporated to achieve high efficiency during wide speed range operation. However, the topology requires changing the direction of LCF magnets which needs accurate control. Recently, a wound-field pole changing vernier machine with distributed winding has been proposed for wide speed range operation [49]. However, the torque ripple of the machine is high and there is no experimental validation. Moreover, the efficiency is low and wide speed range operation of the machine is limited.

This paper proposes a wound-field pole-changing vernier machine with fractional-slot concentrated winding for EV application. The nature of the machine can be changed from a vernier to a wound-field synchronous machine by changing the number of poles. The originality of the proposed topology is that it avoids the above discussed issues of PM pole changing vernier machine and wound field pole changing vernier machine which were presented earlier. Furthermore, none of these manuscripts have experiment results. This paper validates the topology through experiment as well. Section II elaborates the topology, working principle and the pole-changing method of the proposed machine. The electromagnetic performance of the proposed topology in the two operating modes using finite element analysis (FEA) is shown in section III. This section also presents the wide-speed range analysis including the torque-speed and efficiency curve of the machine. Section IV presents the prototype construction and experiment results for validating the proposed idea. Section V concludes the paper.

II. MOTOR TOPOLOGY, POLE CHANGING METHOD AND WORKING PRINCIPLE

A. TOPOLOGY AND WINDING CONFIGURATION

The proposed topology is shown in Fig. 1. It artfully combines the design criteria of a vernier machine and a wound-field synchronous machine. Consequently, it inherits the corresponding machine characteristics of a vernier and a wound-field synchronous machine in its respective modes. It is an outer rotor topology and therefore it can be directly coupled to an EV wheel for direct drive. The proposed machine differs from the PM vernier machine in that it uses dc field windings on the outer rotor to produce a controllable magnetic field. The current direction in the field winding is reversed which also reverses the rotor magnetic field.

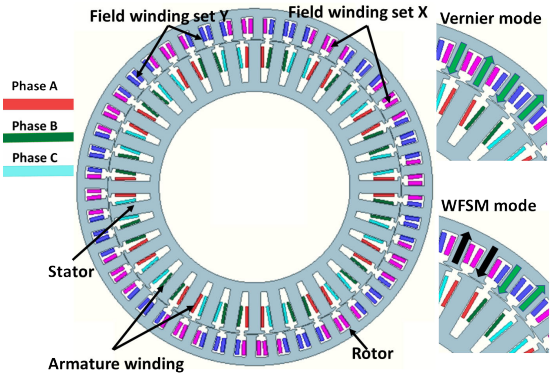

FIGURE 1. Configuration of proposed topology.

There are two sets of field windings on the rotor: X and Y. Each set has 24 coils wound on individual rotor teeth. All the coils in X are connected in series. Similarly, all the coils in Y are connected in series separately. There are two sets of brushes and slip rings. The first set is to provide current to field winding set X and the second set is used to provide current to field winding set Y. The stator is equipped with a 3-phase concentrated armature winding. The short end winding length limits the stator copper losses due to its concentrated winding.

B. POLE CHANGING METHOD

A special circuit is utilized for the pole-changing operation as shown in Fig. 2. Both field winding sets are connected in the circuit. The direction of dc current in the winding set X can be changed by controlling the switches. In one mode S1 and S4 stay on whereas S2 and S3 stay off. To change direction of field winding X current, condition of switches is reversed (S1, S4 off and S2, S3 on). The switches S5-S6 control the winding set Y, which does not need to change direction.

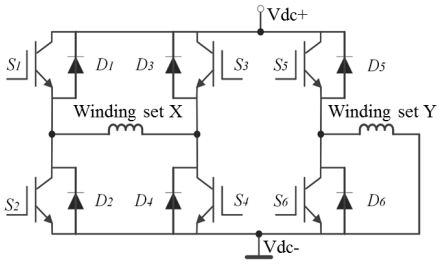

FIGURE 2. Circuit for pole changing operation.

C. OPERATING PRINCIPLE

The proposed machine works as vernier as well as wound-field synchronous machine (WFSM). For the machine to work in the two modes, the machine must satisfy (1) and (2):

$$Z_r = Z_s - P \tag{1}$$

$$Z_r > P \tag{2}$$

where Z_r, Z_s and P represent the number of rotor pole pairs, stator slots, and armature pole pairs, respectively. Equation (1) defines the basic characteristic of a vernier machine. This must be fulfilled for the proposed machine to work in the vernier mode. Equation (2) demands that the pole pairs of the rotor be more than the stator pole pairs so that they can be reduced to armature pole pairs, hence, using the advantages of pole changing. By satisfying (2), the frequency of the armature current is reduced, which decreases the core losses and, hence, improves the efficiency of the machine. To satisfy the above design criteria, the rotor field winding is divided into two sets of windings, that is, X and Y. The pole ratio (PR) of the machine is decided based on (3):

$$Z_r/P = PR \tag{3}$$

If $PR = 2$, the number coils in winding set X and Y are equal. With $PR = 2$, the frequency of the armature in wound-field synchronous mode will be half the value of that in vernier mode. Similarly, if PR is 17, the frequency of the armature winding will be reduced 17 times in the WFSM mode. Table 1 shows some possible slot pole combinations for the wound-field pole-changing vernier machine. In this paper, any slot pole combination with slots per pole per phase <1 is regarded as a fractional-slot concentrated winding, whereas that with slots per pole per phase ≥ 1 is regarded as an overlap winding.

In the vernier mode, the machine satisfies (1); hence, the machine works using the magnetic gearing effect. In this study, Z_r, Z_s and P are chosen as 24, 36 and 12, respectively. Fig. 3(a) shows the airgap flux density in vernier mode, and Fig. 3(b) shows its harmonic spectra. Two main components can be observed in the airgap flux density. The 24 pole pairs

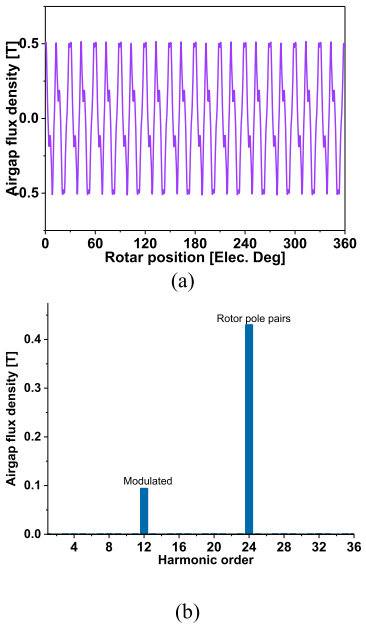

FIGURE 3. Airgap flux density in Vernier mode (a) waveform (b) harmonic spectra.

TABLE 1. Pole slot combination of proposed machine.

Z_s \ Z_r		2	4	5	7	8	-----	24
3	P	1	-	-	-	-	-----	-
	PR	2	-	-	-	-	-----	-
6	P	4	2	1			-----	-
	PR	1/2	2	5			-----	
12	P	-	-	-	-	4	-----	-
	PR	-	-	-	-	2	-----	-
36	P	-	-	-	-	-	-----	12
	PR	-	-	-	-	-	-----	2

component indicates the number of rotor field pole pairs, whereas the component with 12 pole pairs is the result of modulation due to stator slots. This modulation effect causes the rotor to rotate at a specific fraction of the rotating speed of stator field. Hence, the speed of the machine is geared down similar to a magnetic gear. This mechanism causes a small movement of the rotor to produce a large change in the flux, causing vernier machines to have a higher back-EMF than conventional synchronous machines.

For the machine to work in the WFSM mode (4) must be satisfied

$$Z_r = P \tag{4}$$

The current direction in field winding set X is reversed, and the direction of the equivalent magnetic field is changed. Two coils produce flux in the same direction. The total poles of the rotor field winding are reduced from 24 to 12 pole pairs. In the WFSM mode, Fig. 4(a) shows the airgap flux density and Fig. 4(b) shows its harmonics. The airgap can now be observed to show 12 pole pair main component in the airgap flux density. The 12 pole pairs of the rotor interact with the 12 pole pairs of the stator to produce a torque similar to that of a conventional synchronous machine.

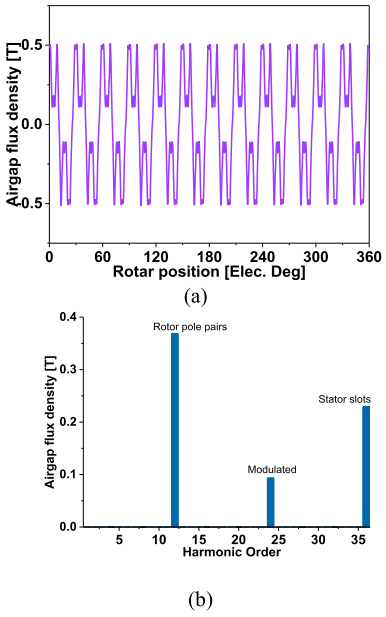

FIGURE 4. Airgap flux density in WFSM mode (a) waveform (b) harmonic spectra.

III. DESIGN CONSIDERATIONS AND PERFORMANCE EVALUATION IN THE TWO MODE

A. DESIGN CONSIDERATIONS

Since the proposed machine has the nature of a vernier machine as well as a conventional wound field synchronous machine, therefore, the well-known D^2L method has been used to design the machine. The pole slot selection for the proposed machine is a difficult choice and must be conducted carefully. If the number of rotor pole pairs are chosen to be much greater in comparison to the number of stator pole pairs, machine will have a much higher efficiency in the vernier mode. Moreover, the machine will have a higher torque density in the vernier mode. However, the drawbacks are higher cogging torque and harmonics in back EMF in WFSM mode. A high torque ripple is undesirable in applications such as EVs, leading to a tradeoff between a high torque ripple and high efficiency. Therefore, the stator pole pairs are selected to be exactly half of the rotor pole pairs. In this case, the ripple of the machine is not very high, and the efficiency of the machine is adequate during the wide speed rang operation. The power of the machine was decided to be around 900 W in order to validate the proposed topology. Considering EV application, the stack length of the proposed machine was initially designed to be 60 mm. Using the general sizing equations, all the parameters such as airgap diameter, number of turns, stator current etc. were determined. Then based on finite element method (FEM) simulations, the parameters were finalized.

Moreover, the split ratio (ratio of the rotor's inner diameter to its outer diameter) has also been examined during the machine design. A higher torque usually results from a higher split ratio. However, the fill factor of the rotor field winding and saturation of the rotor core limits the value of split ratio. Therefore, with a fixed outer machine diameter, this value cannot be increased beyond a specified value. A split ratio of 0.8 was finalized during the design of proposed topology.

Open stator slots are usually selected for vernier machines because they are known to produce a higher modulation effect and, hence, a higher torque density. On the other hand, semi-closed slots are usually selected for wound-field synchronous machines, because they are known to produce lower cogging torque. In the proposed machine, the cogging torque is significant in the WFSM mode, contributing to torque ripple as well. Therefore, to limit the cogging torque, semi-closed slots were selected in the final machine design. Table 2 shows the main parameters of the final designed machine.

TABLE 2. Main parameters of proposed machine.

Item	Unit	Value
Rotor outer diameter	mm	306
Rotor inner diameter	mm	253
Stator outer diameter	mm	252
Stator inner diameter	mm	164
Stack length	mm	65
Base speed	rpm	300
Stator current	A	4
Field winding current	A	3.5
Stator fill factor	%	47
Rotor fill factor	%	46
Stator current density	A/mm^2	2.1
Rotor current density	A/mm^2	5.3
Stator coil diameter (AWG)	mm	1.62(14)
Rotor coil diameter (AWG)	mm	0.9(19)

B. PERFORMANCE EVALUATION IN TWO MODES

The electromagnetic characteristics of the machine are investigated using FEA and compared in two modes. Figs. 5 and 6 show comparison of flux linkages in the two modes, respectively. The flux linkage of the vernier mode is lower due to its higher leakage flux caused by the large number of rotor pole pairs. Figs. 7 and 8 show the back-EMF of the proposed machine in the two modes. An rms value of 65 V is obtained in the vernier mode compared to 43 V in the WFSM mode. In both modes, field current of 3.5 A is used. Vernier mode has higher back EMF due to its vernier effect. Moreover, the back EMF of the vernier mode is more sinusoidal than that of the WFSM mode. Sinusoidal back EMF is an inherent quality of vernier machines.

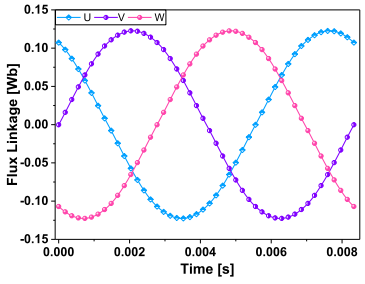

FIGURE 5. Flux linkage Vernier mode.

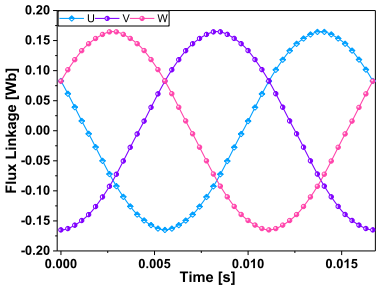

FIGURE 6. Flux linkage WFSM mode.

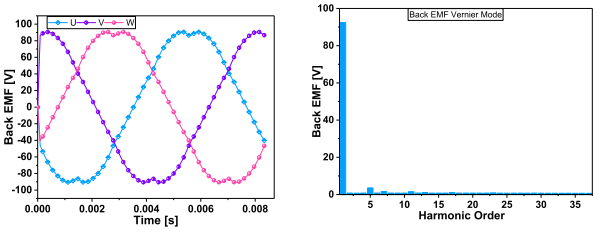

FIGURE 7. Back EMF Vernier mode (a) waveform (b) harmonic spectra.

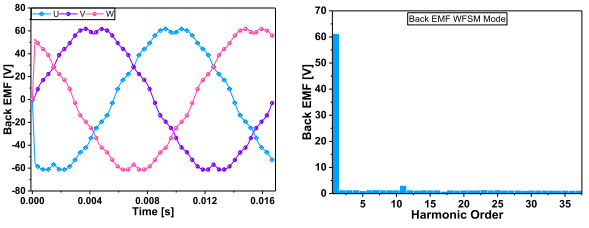

FIGURE 8. Back EMF WFSM mode (a) waveform (b) harmonic spectra.

Fig. 9 and Fig.10 show the no-current torque of the machine in the two modes. Here, only field current is applied and there is no stator current. The no-current torque is equivalent to cogging torque in PM machine. The vernier mode

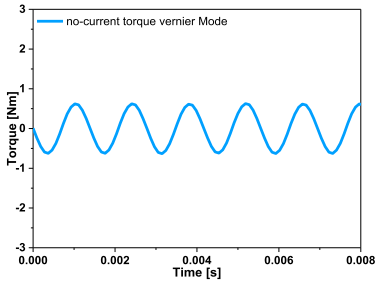

FIGURE 9. No-current torque Vernier mode.

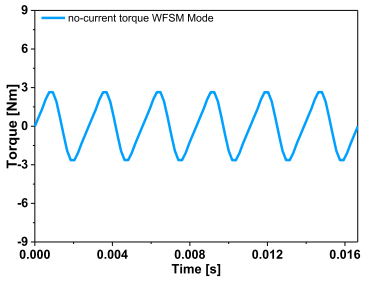

FIGURE 10. No-current torque WFSM mode.

has a lower no-current torque than the WFSM mode. The low no-current torque is caused by the higher number of rotor pole pairs.

Figs. 11 and Fig. 12 depict the torque in the two modes, respectively. An average torque of 28.6 Nm with a ripple of 7% is obtained in the vernier mode. An average torque of 18.9 Nm with a ripple of 24% is obtained in the WFSM mode. The WFSM mode has higher torque ripple due to its higher no-current torque and additional harmonics in the back-EMF.

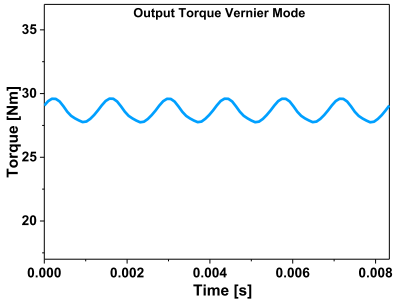

FIGURE 11. Output torque Vernier mode.

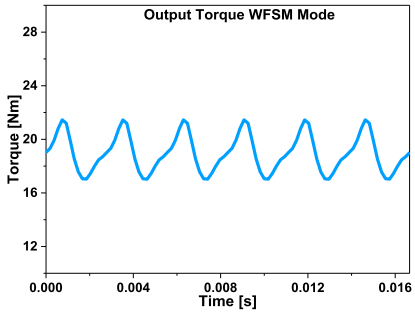

FIGURE 12. Output torque WFSM mode.

Furthermore, the dynamic performance of the proposed machine has also been analyzed using commercial FEA package JMAG version 17. Fig. 13 shows the dynamic response of the machine when a full load of 28 Nm is attached to the machine. Based on the inertia, load torque and damping constant, the proposed machine takes about 3 seconds to reach the synchronous speed.

The phase voltages of the proposed machine are compared in the two modes in Fig. 14 and Fig. 15. The vernier mode

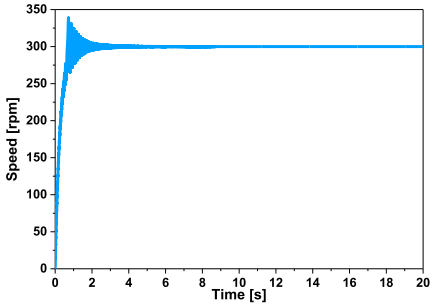

FIGURE 13. Dynamic simulation of proposed machine.

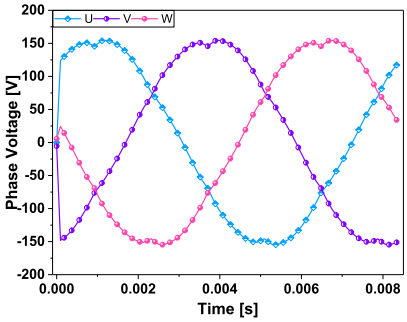

FIGURE 14. Phase voltages vernier mode.

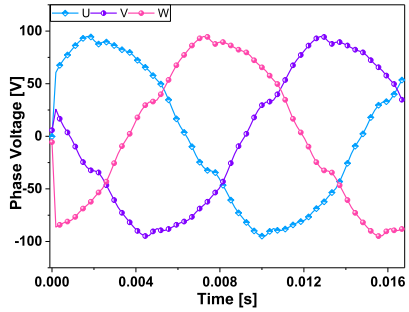

FIGURE 15. Phase voltages WFSM mode.

has higher phase voltages than the WFSM mode. This can be explained by the higher back-EMF as well as higher inductive voltage drop of the vernier mode.

C. WIDE SPEED RANGE ANALYSIS

The wide speed range operation of the proposed machine is initially analyzed using FEA. First the machine is analyzed in each mode separately to elaborate the advantages and limitations of each mode during wide speed range operation. Three types of control have been used to increase the speed of the machine in each mode, that is, field current control, armature current control and d-axis current control. The torque- speed and efficiency curves of the proposed machine in the vernier and WFSM mode are shown in Fig. 16. Vernier mode has higher torque and higher efficiency from 0-300 rpm whereas the WFSM mode has higher efficiency beyond 300 rpm. The vernier mode has a lower efficiency due to its higher core losses after 300 rpm. The WFSM mode has better

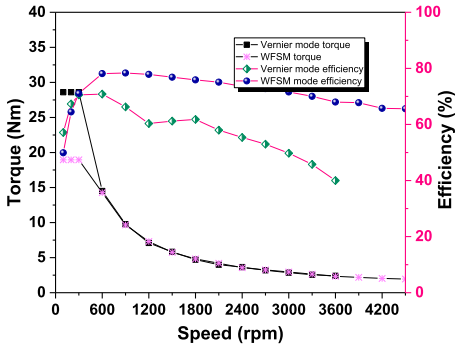

FIGURE 16. Torque-speed and efficiency curve.

efficiency at higher speeds due to its comparatively lower frequency which limits the core losses in this mode. Moreover, the maximum speed of the vernier mode is observed to be 3600 rpm whereas that in the WFSM mode is 4500 rpm. The speed range of WFSM mode is extended due to its lower phase voltages. For continuous operation of the proposed machine in EV application, 600 rpm is selected to be the optimum point for pole-changing operation. This is because the advantages of vernier machines are utilized until this speed. Beyond this speed, the efficiency starts degrading significantly. Therefore, the machine is proposed to be switched into the WFSM mode beyond this speed to limit the efficiency degradation.

IV. EXPERIMENTAL VALIDATION

A. A PROTOTYPE OF THE PROPOSED MOTOR

The proposed topology was verified by manufacturing a prototype. A single stator and rotor lamination of the machine are shown in Fig. 17 (a). The completed stator is shown in Fig 17 (b). The final completed rotor of the manufactured machine is depicted in Fig. 17 (c). The two sets of field windings X and Y are connected to two separate slip rings. The setup for the experiment of proposed machine is shown in Fig. 17 (d), including a dc power supply for field winding, a dc power supply for the inverter, a digital signal processing (DSP) board, an inverter, the prototype machine, a load machine, a torque transducer, an oscilloscope for monitoring the results, and a system to run the DSP code.

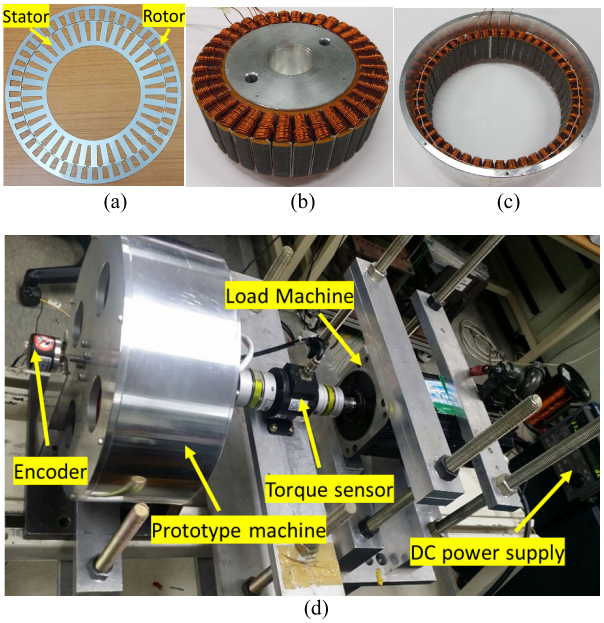

FIGURE 17. Experiment setup (a) Rotor and stator lamination (b) Complete stator with winding (c) Complete rotor with winding (d) Test bed.

B. EXPERIMENTAL RESULTS AND DISCUSSION

1) BACK-EMF IN TWO MODES

Initially, the motor was tested under a no-load condition to confirm the back-EMF of the machine in the two modes. The machine was tested at low ratings with available resources in the lab. The prototype was rotated using an induction machine. The open circuit 3-phase FEM predicted and measured back-EMF comparison in the vernier mode is shown in Fig. 18 (a) and 18(b), respectively. An rms value of 36 V and 35.4 V was obtained in FEM and experiment, respectively. The field current was 2 A in this condition. The machine was then tested in the WFSM mode. The FEM predicted and measured open-circuit 3-phase back-EMF in the WFSM mode is depicted in Fig. 19 (a) and Fig. 19 (b), respectively. Under the same field winding current of 2 A, an rms value of 24 V back-EMF was predicted by FEM. A similar value has measured in test results.

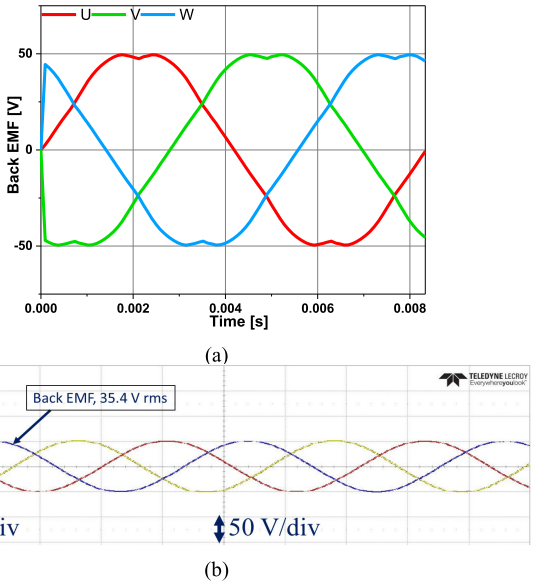

FIGURE 18. Back EMF in vernier mode (a) FEM (b) Measured.

2) OUTPUT TORQUE IN TWO MODES

The output torque of the prototype machine was measured in the two modes by connecting it to a torque transducer and

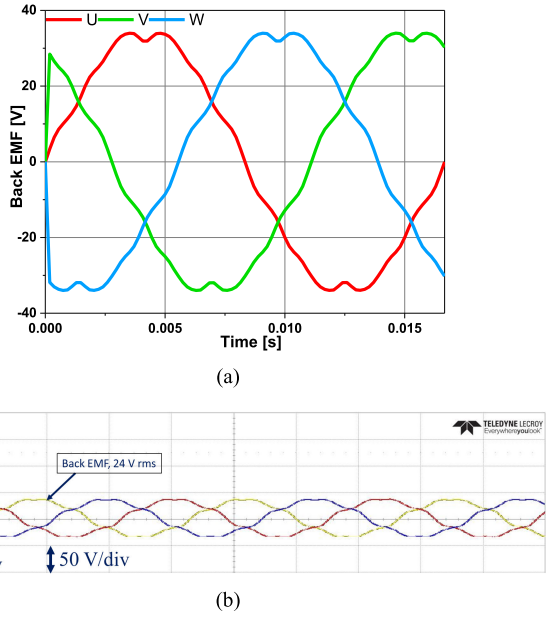

FIGURE 19. Back EMF in WFSM mode (a) FEM (b) Measured.

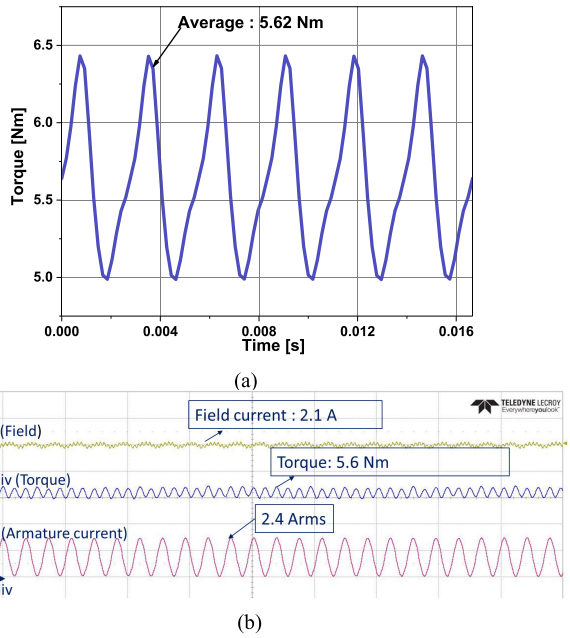

FIGURE 21. Torque in WFSM mode (a) FEM (b) Measured.

a load machine. The 3-phase terminals of the load machine were connected to load resistors. The machine was initially tested in the vernier mode. The FEM predicted torque of the machine is shown in Fig. 20 (a). The measured output torque of the machine along with the applied phase current for the armature winding and field current for the field windings are shown in Fig. 20 (b). An output torque of 8.4 Nm and 8.35 Nm was obtained in FEM and experiment, respectively. The machine was then tested in the WFSM mode at the base speed of 300 rpm under the same conditions. The FEM predicted and measured output torque comparison of the machine in WFSM mode is shown in Fig. 21 (a) and Fig. 21 (b), respectively. An average output torque of 5.62 Nm was predicted by FEM whereas 5.6 Nm was measured during the experiment. Therefore, a close match was found in both modes in no load as well as load analysis.

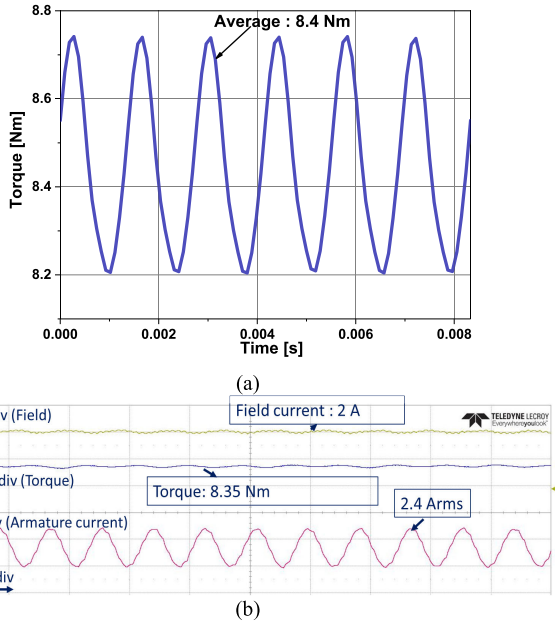

FIGURE 20. Torque in vernier mode (a) FEM (b) Measured.

3) TRANSIENT ANALYSIS

The previously shown results were measured at 300 rpm while the machine was switched from the vernier mode to the WFSM mode in the offline condition. However, the machine was also switched from one mode to another in the online condition so that transient analysis could be performed. The change in the back-EMF of the machine while switching the machine from the vernier to WFSM mode is shown in Fig. 22. A transient of around 20 ms was seen to occur when the machine was switched. Moreover, the frequency of the back EMF reduced to half after switching. Similarly, to analyze the transients the machine was switched from the WFSM to vernier mode in the online condition. The change in the back-EMF can be seen in Fig. 23. A similar transient was found in both cases. This was expected when the machine

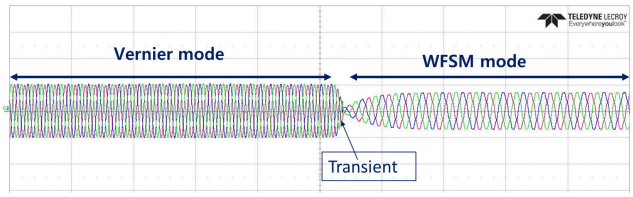

FIGURE 22. Measured back EMF vernier to WFSM mode (transient).

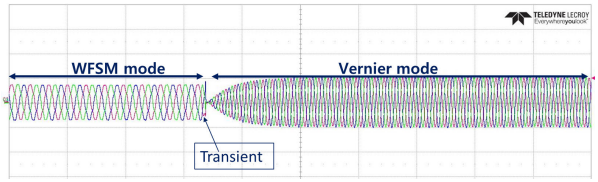

FIGURE 23. Measured back EMF WFSM to vernier mode (transient).

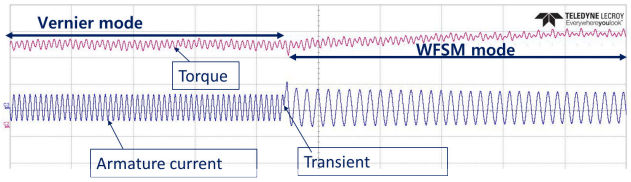

FIGURE 24. Measured torque vernier to WFSM mode (transient).

switched from high to low speed. Because of mode switching, a small transient in the torque was also seen as depicted in Fig. 24. When the machine switched from the vernier to WFSM mode, the current of the machine was observed to increase, which increased the torque of the machine. This is because in the WFSM mode, the back-EMF of the machine decreases thus increasing the difference between input voltages and back EMF of the machine. Hence, a large current flow in the windings of the machine, which increases the torque of the machine. This was caused by the non-flexible load attached to the machine. Similarly, the transient also occurred when the machine was switched from WFSM to vernier mode as depicted in Fig. 25. This time, the currents of the machine decreased and therefore torque of the machine decreased. This occurred because in the vernier mode, the back-EMF of the machine increased, in turn decreasing the difference between input voltages and back-EMF. Hence, the current drawn by the windings decreased, resulting in decreased torque. This is also caused by the same non-flexible load attached to the machine.

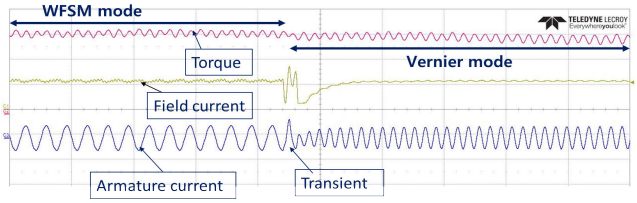

FIGURE 25. Measured torque WFSM mode to vernier mode (transient).

4) WIDE SPEED RANGE ANALYSIS DURING THE EXPERIMENT

The prototype machine was also tested for wide speed range analysis. In the vernier mode at a base speed of 300 rpm, the Vdc required by the inverter was found to be 146 V. This voltage was assumed to be the inverter limit. The machine was then switched to the WFSM mode at 600 rpm. The machine was then tested for wide speed range using negative d-axis current while remaining in WFSM mode. The required torque and speeds were achieved, and a constant power was obtained. Moreover, the Vdc applied to the inverter remained fixed during this operation. The FEM predicted and measured torque-speed curves of the proposed machine are compared in Fig. 26. Table 3 summarizes the overall comparison of the FEM and measured results. For efficiency measurement in experiment, the copper losses of the machine were measured by measuring the winding resistance (field and armature) from the actual prototype whereas iron losses of the machine were assumed to be same as FEM. Low torque ripple was found during experiment in comparison to the FEM results. The estimated cause is the high inertia of the machine.

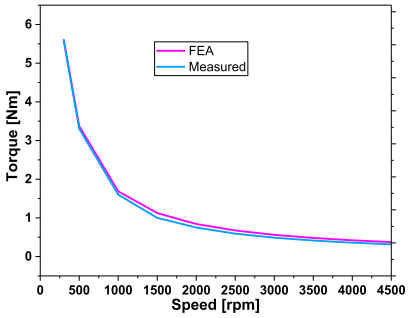

FIGURE 26. Comparison of measured and simulated torque speed curve.

TABLE 3. Comparison of FEM and experimental results.

Item	Unit	Vernier mode		WFSM mode	
		FEM	Experiment	FEM	Experiment
Back EMF	V	36	35.4	24	24
Torque	Nm	8.4	8.35	5.62	5.6
Torque ripple	%	6.35	6	24	21
Efficiency	%	68.6	67	68.9	66.5

V. CONCLUSION

This paper proposed a wound-field pole-changing vernier machine for application in electric vehicles. It demonstrates that the merits of two machines that is vernier machine and wound-field synchronous machine can be obtained in a single topology using the proposed pole-changing method. The method of pole changing using a special circuit was described. The machine was initially analyzed using FEM. The finite element results of the machine were validated by comparing them with experimental results, which proved that the proposed machine can run in the two modes. Although two sets of brushes and slip rings are required in the proposed machine, brushes with new materials have been developed which do not require frequent maintenance. Furthermore, the proposed machine also possesses the advantage of smooth switching from combustion engine to EV mode in hybrid

electric vehicles. This is because, field winding current can be turned off at the time of switching and therefore, there no back EMF will be induced in the armature winding of the machine. Hence, the proposed machine is a good candidate for EV application.

REFERENCES

[1] A. Emadi, Y. Joo Lee, and K. Rajashekara, "Power electronics and motor drives in electric, hybrid electric, and plug-in hybrid electric vehicles," *IEEE Trans. Ind. Electron.*, vol. 55, no. 6, pp. 2237–2245, Jun. 2008, doi: 10.1109/TIE.2008.922768.

[2] A. Y. Saber and G. K. Venayagamoorthy, "Plug-in vehicles and renewable energy sources for cost and emission reductions," *IEEE Trans. Ind. Electron.*, vol. 58, no. 4, pp. 1229–1238, Apr. 2011, doi: 10.1109/TIE.2010.2047828.

[3] K. T. Chau, *Electric Vehicle Machines and Drives: Design, Analysis and Application*. Hoboken, NJ, USA: Wiley, 2015.

[4] C. C. Chan and K. T. Chau, "An overview of power electronics in electric vehicles," *IEEE Trans. Ind. Electron.*, vol. 44, no. 1, pp. 3–13, Feb. 1997, doi: 10.1109/41.557493.

[5] M. Terashima, T. Ashikaga, T. Mizuno, K. Natori, N. Fujiwara, and M. Yada, "Novel motors and controllers for high-performance electric vehicle with four in-wheel motors," *IEEE Trans. Ind. Electron.*, vol. 44, no. 1, pp. 28–38, Feb. 1997, doi: 10.1109/41.557496.

[6] K. T. Chau, C. C. Chan, and C. Liu, "Overview of permanent-magnet brushless drives for electric and hybrid electric vehicles," *IEEE Trans. Ind. Electron.*, vol. 55, no. 6, pp. 2246–2257, Jun. 2008, doi: 10.1109/TIE.2008.918403.

[7] C. C. Chan, K. T. Chau, J. Z. Jiang, W. Xia, M. Zhu, and R. Zhang, "Novel permanent magnet motor drives for electric vehicles," *IEEE Trans. Ind. Electron.*, vol. 43, no. 2, pp. 331–339, Apr. 1996, doi: 10.1109/41.491357.

[8] Z. Chen, B. Wang, Z. Chen, and Y. Yan, "Comparison of flux regulation ability of the hybrid excitation doubly salient machines," *IEEE Trans. Ind. Electron.*, vol. 61, no. 7, pp. 3155–3166, Jul. 2014, doi: 10.1109/TIE.2013.2281171.

[9] Z. Chen and N. Zhou, "Flux regulation ability of a hybrid excitation doubly salient machine," *IET Electr. Power Appl.*, vol. 5, no. 2, p. 224, 2011, doi: 10.1049/iet-epa.2010.0072.

[10] W. Hua, P. Su, M. Tong, and J. Meng, "Investigation of a five-phase E-Core hybrid-excitation flux-switching machine for EV and HEV applications," *IEEE Trans. Ind. Appl.*, vol. 53, no. 1, pp. 124–133, Jan. 2017, doi: 10.1109/TIA.2016.2608324.

[11] H. Yang, H. Lin, Z. Q. Zhu, D. Wang, S. Fang, and Y. Huang, "A variable-flux hybrid-PM switched-flux memory machine for EV/HEV applications," *IEEE Trans. Ind. Appl.*, vol. 52, no. 3, pp. 2203–2214, May 2016, doi: 10.1109/TIA.2016.2524400.

[12] Y. Gao, D. Li, R. Qu, X. Fan, J. Li, and H. Ding, "A novel hybrid excitation flux reversal machine for electric vehicle propulsion," *IEEE Trans. Veh. Technol.*, vol. 67, no. 1, pp. 171–182, Jan. 2018, doi: 10.1109/TVT.2017.2750206.

[13] Y. Gao, R. Qu, D. Li, J. Li, and G. Zhou, "Consequent-pole flux-reversal permanent-magnet machine for electric vehicle propulsion," *IEEE Trans. Appl. Supercond.*, vol. 26, no. 4, Jun. 2016, Art. no. 5200105, doi: 10.1109/TASC.2016.2514345.

[14] Y. Hu, S. Zhu, C. Liu, and K. Wang, "Electromagnetic performance analysis of interior PM machines for electric vehicle applications," *IEEE Trans. Energy Convers.*, vol. 33, no. 1, pp. 199–208, Mar. 2018, doi: 10.1109/TEC.2017.2728689.

[15] M. Olszewski, "Evaluation of the 2010 Toyota Prius hybrid synergy drive system," U.S. Dept. Energy, Vehicle Technol., Washington, DC, USA, Tech. Rep. 20585-0121, Mar. 2011, pp. 43–48.

[16] K. I. Laskaris and A. G. Kladas, "Internal permanent magnet motor design for electric vehicle drive," *IEEE Trans. Ind. Electron.*, vol. 57, no. 1, pp. 138–145, Jan. 2010, doi: 10.1109/TIE.2009.2033086.

[17] V. Ostovic, "Pole-changing permanent-magnet machines," *IEEE Trans. Ind. Appl.*, vol. 38, no. 6, pp. 1493–1499, Nov. 2002, doi: 10.1109/TIA.2002.805568.

[18] F. Li, K. T. Chau, and C. Liu, "Pole-changing flux-weakening DC-excited dual-memory machines for electric vehicles," *IEEE Trans. Energy Convers.*, vol. 31, no. 1, pp. 27–36, Mar. 2016, doi: 10.1109/TEC.2015.2479458.

[19] D. Wang, H. Lin, H. Yang, Y. Zhang, and X. Lu, "Design and analysis of a variable-flux pole-changing permanent magnet memory machine," *IEEE Trans. Magn.*, vol. 51, no. 11, Nov. 2015, Art. no. 8113004, doi: 10.1109/TMAG.2015.2448118.

[20] R. Dutta and M. F. Rahman, "Design and analysis of an interior permanent magnet (IPM) machine with very wide constant power operation range," *IEEE Trans. Energy Convers.*, vol. 23, no. 1, pp. 25–33, Mar. 2008, doi: 10.1109/TEC.2007.905061.

[21] I. Boldea, L. N. Tutelea, L. Parsa, and D. Dorrell, "Automotive electric propulsion systems with reduced or no permanent magnets: An overview," *IEEE Trans. Ind. Electron.*, vol. 61, no. 10, pp. 5696–5711, Oct. 2014, doi: 10.1109/TIE.2014.2301754.

[22] A. V. Sant, V. Khadkikar, W. Xiao, and H. H. Zeineldin, "Four-axis vector-controlled dual-rotor PMSM for plug-in electric vehicles," *IEEE Trans. Ind. Electron.*, vol. 62, no. 5, pp. 3202–3212, May 2015, doi: 10.1109/TIE.2014.2387094.

[23] S. Chung, S. Moon, D. Kim, and J. Kim, "Development of a 20-pole–24-slot SPMSM with consequent pole rotor for in-wheel direct drive," *IEEE Trans. Ind. Electron.*, vol. 63, no. 1, pp. 302–309, Jan. 2016, doi: 10.1109/TIE.2015.2472375.

[24] H. Cai, B. Guan, and L. Xu, "Low-cost ferrite PM-assisted synchronous reluctance machine for electric vehicles," *IEEE Trans. Ind. Electron.*, vol. 61, no. 10, pp. 5741–5748, Oct. 2014, doi: 10.1109/TIE.2014.2304702.

[25] S. J. Galioto, P. B. Reddy, A. M. EL-Refaie, and J. P. Alexander, "Effect of magnet types on performance of high-speed spoke Interior-Permanent-Magnet machines designed for traction applications," *IEEE Trans. Ind. Appl.*, vol. 51, no. 3, pp. 2148–2160, May 2015, doi: 10.1109/TIA.2014.2375380.

[26] C. H. T. Lee, K. T. Chau, and C. Liu, "Design and analysis of an electronic-geared magnetless machine for electric vehicles," *IEEE Trans. Ind. Electron.*, vol. 63, no. 11, pp. 6705–6714, Nov. 2016, doi: 10.1109/TIE.2016.2582793.

[27] T. Wang, P. Zheng, Q. Zhang, and S. Cheng, "Design characteristics of the induction motor used for hybrid electric vehicle," *IEEE Trans. Magn.*, vol. 41, no. 1, pp. 505–508, Jan. 2005, doi: 10.1109/TMAG.2004.838967.

[28] W. Ding, G. Liu, and P. Li, "A hybrid control strategy of hybrid-excitation switched reluctance motor for torque ripple reduction and constant power extension," *IEEE Trans. Ind. Electron.*, vol. 67, no. 1, pp. 38–48, Jan. 2020, doi: 10.1109/TIE.2019.2891467.

[29] M. Takeno, A. Chiba, N. Hoshi, S. Ogasawara, M. Takemoto, and M. A. Rahman, "Test results and torque improvement of the 50-kW switched reluctance motor designed for hybrid electric vehicles," *IEEE Trans. Ind. Appl.*, vol. 48, no. 4, pp. 1327–1334, Jul. 2012, doi: 10.1109/TIA.2012.2199952.

[30] W. Q. Chu, Z. Q. Zhu, J. Zhang, X. Liu, D. A. Stone, and M. P. Foster, "Investigation on operational envelops and efficiency maps of electrically excited machines for electrical vehicle applications," *IEEE Trans. Magn.*, vol. 51, no. 4, pp. 1–10, Apr. 2015, doi: 10.1109/TMAG.2014.2359008.

[31] C. H. T. Lee, K. T. Chau, and C. Liu, "Design and analysis of a cost-effective magnetless multiphase flux-reversal DC-field machine for wind power generation," *IEEE Trans. Energy Convers.*, vol. 30, no. 4, pp. 1565–1573, Dec. 2015, doi: 10.1109/TEC.2015.2443155.

[32] D. Dorrell, L. Parsa, and I. Boldea, "Automotive electric motors, generators, and actuator drive systems with reduced or no permanent magnets and innovative design concepts," *IEEE Trans. Ind. Electron.*, vol. 61, no. 10, pp. 5693–5695, Oct. 2014.

[33] D. G. Dorrell, "Are wound-rotor synchronous motors suitable for use in high efficiency torque-dense automotive drives?" in *Proc. 38th Annu. Conf. IEEE Ind. Electron. Soc. (IECON)*, Montreal, QC, Canada, Oct. 2012, pp. 4880–4885, doi: 10.1109/IECON.2012.6389578.

[34] J. K. Noland, S. Nuzzo, A. Tessarolo, and E. F. Alves, "Excitation system technologies for wound-field synchronous machines: Survey of solutions and evolving trends," *IEEE Access*, vol. 7, pp. 109699–109718, 2019, doi: 10.1109/ACCESS.2019.2933493.

[35] K. Groth, F. Heidenfelder, and R. Holinski, "Advancements of tribological performance of carbon brushes in electrical motors," *Ind. Lubrication Tribol.*, vol. 53, no. 1, pp. 5–10, Feb. 2001.

[36] G. Toth, J. Mäklin, N. Halonen, J. Palosaari, J. Juuti, H. Jantunen, K. Kordas, W. G. Sawyer, R. Vajtai, and P. M. Ajayan, "Carbon-nanotube-based electrical brush contacts," *Adv. Mater.*, vol. 21, no. 20, pp. 2054–2058, May 2009.

[37] Q. Ali, T. A. Lipo, and B.-I. Kwon, "Design and analysis of a novel brushless wound rotor synchronous machine," *IEEE Trans. Magn.*, vol. 51, no. 11, pp. 1–4, Nov. 2015, doi: 10.1109/TMAG.2015.2440433.
[38] G. Jawad, Q. Ali, T. A. Lipo, and B.-I. Kwon, "Novel brushless wound rotor synchronous machine with zero-sequence third-harmonic field excitation," *IEEE Trans. Magn.*, vol. 52, no. 7, Jul. 2016, Art. no. 8106104, doi: 10.1109/TMAG.2015.2512281.
[39] A. Frias, P. Pellerey, A. K. Lebouc, C. Chillet, V. Lanfranchi, G. Friedrich, L. Albert, and L. Humbert, "Rotor and stator shape optimization of a synchronous machine to reduce iron losses and acoustic noise," in *Proc. IEEE Vehicle Power Propuls. Conf.*, Oct. 2012, pp. 98–103, doi: 10.1109/VPPC.2012.6422572.
[40] W. Liu and T. A. Lipo, "Analysis of consequent pole spoke type Vernier permanent magnet machine with alternating flux barrier design," *IEEE Trans. Ind. Appl.*, vol. 54, no. 6, pp. 5918–5929, Nov. 2018, doi: 10.1109/TIA.2018.2856579.
[41] X. Ren, D. Li, R. Qu, Z. Yu, and Y. Gao, "Investigation of spoke array permanent magnet Vernier machine with alternate flux bridges," *IEEE Trans. Energy Convers.*, vol. 33, no. 4, pp. 2112–2121, Dec. 2018, doi: 10.1109/TEC.2018.2846259.
[42] D. Li, T. Zou, R. Qu, and D. Jiang, "Analysis of fractional-slot concentrated winding PM Vernier machines with regular open-slot stators," *IEEE Trans. Ind. Appl.*, vol. 54, no. 2, pp. 1320–1330, Mar. 2018, doi: 10.1109/TIA.2017.2778686.
[43] T. Zou, D. Li, R. Qu, D. Jiang, and J. Li, "Advanced high torque density PM Vernier machine with multiple working harmonics," *IEEE Trans. Ind. Appl.*, vol. 53, no. 6, pp. 5295–5304, Nov. 2017, doi: 10.1109/TIA.2017.2724505.
[44] B. Kim and T. A. Lipo, "Operation and design principles of a PM Vernier motor," *IEEE Trans. Ind. Appl.*, vol. 50, no. 6, pp. 3656–3663, Nov. 2014, doi: 10.1109/TIA.2014.2313693.
[45] C. Liu, J. Zhong, and K. T. Chau, "A novel flux-controllable Vernier permanent-magnet machine," *IEEE Trans. Magn.*, vol. 47, no. 10, pp. 4238–4241, Oct. 2011, doi: 10.1109/TMAG.2011.2152374.
[46] H. Wang, S. Fang, H. Yang, H. Lin, D. Wang, Y. Li, and C. Jiu, "A novel consequent-pole hybrid excited Vernier machine," *IEEE Trans. Magn.*, vol. 53, no. 11, Nov. 2017, Art. no. 8112304, doi: 10.1109/TMAG.2017.2695494.
[47] A. Arif, N. Baloch, and B. I. Kwon, "Wide speed range operation of permanent magnet Vernier machines," *Electron. Lett.*, vol. 54, no. 18, pp. 1070–1072, Sep. 2018, doi: 10.1049/el.2018.5008.
[48] N. Baloch and B.-I. Kwon, "A pole changing Vernier machine with consequent pole rotor," *Int. J. Appl. Electromagn. Mech.*, vol. 59, no. 3, pp. 931–941, Mar. 2019.
[49] N. Baloch and B.-I. Kwon, "A distributed winding wound field pole-changing Vernier machine for variable speed application," *IEEE Trans. Magn.*, vol. 55, no. 7, Jul. 2019, Art. no. 8203706, doi: 10.1109/TMAG.2019.2900470.

NOMAN BALOCH was born in Pakistan. He received the B.S. degree in electronics engineering from the Balochistan University of Information Technology, Engineering and Management Sciences (BUITEMS), Quetta, Pakistan, in 2010, and the Ph.D. degree in electrical and electronic engineering from Hanyang University, South Korea, in February 2020.

From 2010 to 2015, he was a Deputy Assistant Director with the National Database and Registration Authority (NADRA), Pakistan. He is currently a Postdoctoral Research Fellow with the Energy Conversion Laboratory, Hanyang University. His research interest includes design and control of electrical machines.

SHAHID ATIQ was born in Punjab, Pakistan. He received the bachelor's and master's degrees from the University of Engineering and Technology Taxila, Pakistan, and the Ph.D. degree from the Energy Conversion Systems Laboratory, Hanyang University, South Korea. He held different managerial and educational posts with various institutions. He is currently an Associate Professor and the Head of the Department of Electrical Engineering, Khwaja Fareed University of Engineering and Information Technology, Rahim Yar Khan, Pakistan.

BYUNG-IL KWON (Senior Member, IEEE) was born in 1956. He received the B.S. and M.S. degrees in electrical engineering from Hanyang University, Ansan, South Korea, in 1981 and 1983, respectively, and the Ph.D. degree in electrical engineering and machine analysis from The University of Tokyo, Tokyo, Japan, in 1989. From 1989 to 2000, he was a Visiting Researcher with the Faculty of Science and Engineering Laboratory, University of Waseda, Tokyo. In 1990, he was a Researcher with the Toshiba System Laboratory, Yokohama, Japan. In 1991, he was a Senior Researcher with the Institute of Machinery and Materials Magnetic Train Business, Daejeon, South Korea. From 2001 to 2008, he was a Visiting Professor with the University of Wisconsin- Madison, Madison, WI, USA. He is currently a Professor with Hanyang University. His research interest includes design and control of electric machines.